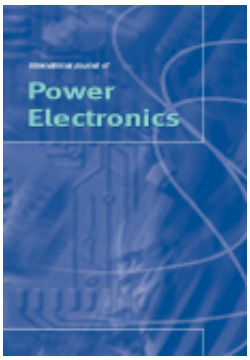

International Journal of Power Electronics

ISSN online: 1756-6398 - ISSN print: 1756-638X
https://www.inderscience.com/ijpelec

Detection and classification of faults in DC microgrids utilising artificial neural network with bidirectional gated recurrent units

Ramaprasanna Dalai, Sarat Chandra Swain

DOI: 10.1504/IJPELEC.2025.10068210

Article History:

Received:	10 May 2024
Last revised:	18 September 2024
Accepted:	19 October 2024
Published online:	15 January 2025

Detection and classification of faults in DC microgrids utilising artificial neural network with bidirectional gated recurrent units

Ramaprasanna Dalai* and
Sarat Chandra Swain

School of Electrical Engineering,
KIIT University,
Patia, Bhubaneswar, Odisha, 751024, India
Email: ramaprasanna213@gmail.com
Email: scswainfel@kiit.ac.in
*Corresponding author

Abstract: This paper proposes a fault detection and classification method for DC-MG. This paper aims to identify and categorise errors with increased precision. In order to improve the detection accuracy, a hybrid artificial neural network (ANN) and bidirectional gated recurrent unit (BiGRU) is proposed. The input signal's features (voltage and current) are extracted using the discrete wavelet transform (DWT). The hybrid ANN-BiGRU model analyses and classifies faults in the microgrid system using the features extracted using the DWT. The osprey optimisation algorithm (OOA) is used to adjust the weight parameters to minimise error. The simulation results were obtained using the MATLAB/Simulink tool. The simulation results indicated that the proposed technique acquired a higher accuracy of 99.65%, precision of 99.60%, and recall of 98.5% compared to other state-of-the-art methods.

Keywords: DC microgrid; DC-MG; osprey optimisation algorithm; OOA; artificial neural network bidirectional gated recurrent unit; ANN-BiGRU; discrete wavelet transform; DWT; renewable energy sources; RESs.

Reference to this paper should be made as follows: Dalai, R. and Swain, S.C. (2025) 'Detection and classification of faults in DC microgrids utilising artificial neural network with bidirectional gated recurrent units', *Int. J. Power Electronics*, Vol. 21, No. 1, pp.1–27.

Biographical notes: Ramaprasanna Dalai received his BTech in Electrical Engineering from BPUT and MTech from SoA University in 2008 and 2012 respectively. Currently, he is a research scholar at School Of Electrical Engineering KIIT, University, and Bhubaneswar. He has published more than 15 of papers in national level journals and conferences. His research interests include power system, DC microgrid, and power electronic and drives.

Sarat Chandra Swain brings a wealth of experience and expertise to his role as a Professor at the School of Electrical Engineering, KIIT Deemed to be University. With a PhD in Electrical Engineering from KIIT University in 2010 and an ME from UCE Burla in 2001, he has dedicated 27 years to the field of teaching and research. Throughout his illustrious career, he has made significant contributions to the academic community. He has authored more than 200 research papers, which have been published in reputed international journals and IEEE conferences indexed in Scopus, Web of Science, and Google Scholars. His research interests span a wide range of topics, including applying

AI techniques, soft computing, FACTS controllers, power system stability improvement, PV modelling, and grid interconnection of photovoltaic solar systems. His commitment to nurturing future scholars is evident in his supervision of more than 11 PhD scholars and 45 MTech scholars to date.

1 Introduction

Renewable energy sources (RESs) are rapidly growing energy sources that help to reduce carbon emissions in the economy (Irfan et al., 2024). RES are environmentally benign, clean, readily available, and cost-free (Moradmand et al., 2021; Jadidi et al., 2020). RES are distinct from fossil fuels such as natural gas, coal, and crude oil. The emission of contaminants or greenhouse gas emissions does not have an impact on the environment (Chowdhury et al., 2021). RESs include variable renewable energy (VRE) technologies, such as wind and solar power, which are characterised by their fluctuating and intermittent output (Sasaki et al., 2022; Khan and Wen, 2021; Wang et al., 2023; Alhanaf et al., 2024). The advancement of photovoltaic (PV) generation continues to depend on the implementation of appropriate regulatory and economic policies in different nations (Deotti et al., 2021). Renewable energy (RE) resources are increasingly being employed in distributed generators (DG) as a means to address challenges such as environmental impacts, increased costs, and transmission losses (Zahraoui et al., 2021). DGs are a type of electric generating that is more varied, smaller in size, bidirectional, intricate, and dynamic. DGs are integrated into distribution networks and are known for their flexibility, sustainability, efficiency, reliability, environmental benefits, security, and reduce negative social impacts. Based on various criteria, DGs aim to minimise energy losses, reduce greenhouse gas emissions, and achieve a balance between energy demand and supply (Taher et al., 2024).

Distributed energy resources (DERs) consist of various components, such as renewable and non-renewable generation, electric vehicles, energy storage, demand-side management technologies, and inverters (Salehimehr et al., 2024). Examples of DER are natural gas turbines, fuel cells, electric automobiles, and EV chargers (Lakshmi et al., 2020). DER has garnered considerable attention in recent years due to its notable economic and technical benefits. The advantages of DER include the decrease of power loss, augmentation of voltage profile, maximising of net savings, improvement of system reliability, and reduction of operational expenses. In the context of distribution networks, DERs are assigned in an efficient manner to maximise benefits (Abdelsalam, 2020). Distribution networks are designed to support the increasing number of active customers and adapt their operations based on different incentive schemes (Pragati et al., 2024). A microgrid (MG) is a term used to describe autonomous clusters of energy storage, loads, and electricity sources that are interconnected with distribution networks via a single coupling point (Grcić et al., 2021; Ali et al., 2021; Cepeda et al., 2020).

According to the literature, the MG can be categorised into three distinct types: DC microgrid (DC-MG), hybrid MG, and AC MG (Modi and Usha, 2023). The adoption of DC-MGs has increased in recent years due to advancements in energy storage, power electronics (PEs), and RE technologies (Saurabh et al., 2024). The efficiency and dependability of DC-MG systems are higher than those of AC systems. Multiple DC-MGs are interconnected with adjacent DC-MGs in order to reduce investment

expenses (Bayati et al., 2021a). DC-MGs play a vital role in a variety of applications, including telecommunications, marine systems, transportation, and traction (Chandra et al., 2020; Khaleefah et al., 2024). Hence, the primary disadvantages in safeguarding the DC-MGs encompass swift fluctuations in fault current rates, restricted timeframe for fault identification and resolution, and enhanced uncertainties of the DG. Identification of faults in DC-MG apparatus can be more challenging due to the influence of fault resistance and lower line impedance. The three typical forms of faults in DC-MGs are pole-to-ground (PG), two PG (2PG), and pole-to-pole (PP) (Sistani et al., 2023).

Evaluating the fault distance after faults is a key component of restoring and maintaining the DC-MG. One fault location uses communication, and the other uses local-based approaches. The communication route amplifies the risk of failure, noise, and expense (Bayati et al., 2021b). The artificial neural networks (ANNs) and convolution neural network (Das et al., 2024) methods are utilised to detect and classify faults. Fault detection is necessary to improve controllability via PE converters and extend the life of the PEs switches by mitigating greater fault current magnitudes. Based on the DC-MG, the derivatives of cable current are used to identify problems (Montoya et al., 2022). Many existing methods for fault detection and classification in DC-MGs may have limitations in terms of accuracy, especially in handling complex fault scenarios or noisy data. Some methods can be computationally intensive, making them unsuitable for real-time applications. There are still several research gaps in the various existing approaches, which are summarised. To address these research gaps, a hybrid ANN-BiGRU technique is introduced for defect detection and classification.

The major contribution of this paper is:

- A novel hybrid approach is proposed that combines ANN and BiGRU to enhance the accuracy of fault detection and classification in DC-MGs.
- The proposed model extracts critical features such as voltage and current using DWT. DWT enables the model to capture both time and frequency domain information, thereby improving fault detection sensitivity, especially in complex scenarios.
- The system's performance is further optimised using the OOA, which fine-tunes the weight parameters of the ANN-BiGRU model. This optimisation process minimises errors and enhances the model's efficiency and robustness.
- The proposed method is validated using the MATLAB/Simulink tool. The simulation results demonstrate superior performance compared to other state-of-the-art methods, achieving an accuracy of 99.65%, precision of 99.60%, and recall of 98.5%.

The organisation of this paper is described as follows: Section 2 describes the literature review for the detection and classification of faults. Section 3 explains the proposed methodology, which includes discrete wavelet transform (DWT)-based feature extraction, ANN, BiGRU and osprey optimisation algorithm (OOA). Section 4 provides the test system of the DC-MG, and the simulation results are described in Section 5. Finally, the conclusion of this work is explained in Section 6.

2 Literature survey

The works that address some of the current techniques for defect detection and classification are displayed below:

Barik (2023) discussed the variational mode decomposition (VMD) for classifying and detecting the faults based on the DC-MG. The VMD was employed to decompose the current signal into different intrinsic modes in order to achieve dependable protection. The classification of faults such as PP, line-to-line (LL), three-phase-line-to-ground (LLLG), line-to-ground (LG), and PG was performed using a neural network based on a stacked autoencoder. The empirical findings indicated that the technique achieved a greater level of categorisation accuracy.

Gajula et al. (2023) assessed the use of a probabilistic technique based on DC-MGs to locate and detect the flaws. The objective of this paper was to quickly identify and detect errors in order to keep the false alarm rate low. To make sure that no fault is missed, an increase in faults was identified using the cumulative sum (CUSUM) statistic. The Kron reduction approach is applied to eliminate the internal nodes. The outcomes demonstrate that the strategy's viability was confirmed using the MG test bed.

The hybrid sensor fault tolerant control (HSFTC) method was developed by Chandra and Mohapatro (2023) and implemented on a DC-MG. The utilisation of the HSFTC method was implemented to efficiently manage sensor errors. The HSFTC is equipped with hardware redundancy and analytical redundancy components to effectively manage faults originating from current and voltage sensors. The HSFTC's performance was assessed utilising the Simulink/MATLAB platform. The simulation findings demonstrated that the HSFTC scheme performed superiorly compared to alternative control methods.

Based on a fake data injection assault, Mao et al. (2024) analysed to estimate the DC-MG system. The distributed Kalman filter was used to estimate the attack states and signals. In order to increase the system's robustness, the compensating mechanism was implemented. The outcomes showed that the method successfully prevented external threats and maintained system stability. However, the system did not consider replay or DoS attacks.

The fault location approach using a multi-terminal radial medium voltage DC (MVDC) MG was first presented by Nougain et al. (2023). Depending on the accessibility of the sensor and communication, various terminals were employed to enhance the reliability of the fault location technique. The use of parameter variation allowed for an examination of the fault site. The algorithm's efficacy was verified through the use of electromagnetic transient DC (EMTDC) and power system computer-assisted design (PSCAD) simulations.

Baloch and Muhammad (2021) suggested a data mining technique for fault classification and detection based on MGs. The fault features were eliminated from the faulted current and voltage signals by pre-processing them using the Hilbert transform. Python was used with the MATLAB/Simulink software environment to test and train the data mining design. The AdaBoost classifier-based logistic regression (ACLR) technique was utilised to detect and categorise faults in MG networks. The method achieved improved precision, and the findings showed that it also offers trustworthy measures for MG protection.

Baloch et al. (2021) conducted an evaluation to identify faults in MGs using data mining and wavelet multi-resolution analysis techniques. Wavelet multi-resolution analysis was used to pre-process the current and voltage signals in order to calculate the total harmonic distortion (THD) of both signals. The findings indicated that the methodology demonstrated proficiency in the classification, identification, and detection of errors within the dataset.

The unsupervised learning technique for defect detection and diagnosis (FDD) based on air handling units (AHU) was devised by Yan et al. (2020). Generative adversarial networks (GANs) were employed to address the issues posed by imbalanced data in the field of FDD. GAN was employed to rebalance the dataset and augment the number of erroneous training samples. The simulation findings indicated that the technique exhibited a much higher level of effectiveness compared to alternative techniques. Nevertheless, the resilience of the approaches was not adequately validated. Table 1 summarises the existing related works conducted by various authors.

Table 1 Overview of existing related works

Author	*Method*	*Advantages*	*Disadvantages*	*Tool*
Barik (2023)	Variational mode decomposition (VMD)	Reliable and fast	High computational complexity	MATLAB/Simulink
Gajula et al. (2023)	Cumulative sum (CUSUM) algorithm	Real-time monitoring	Overhead and complexity	MATLAB/Simulink
Chandra and Mohapatro (2023)	Hybrid sensor fault tolerant control (HSFTC) scheme	Scalability and flexibility	Higher complexity	Simulink/MATLAB
Mao et al. (2024)	Distributed Kalman filter algorithm	Lower latency	Communication overhead	MATLAB
Nougain et al. (2023)	Multi-terminal radial medium voltage DC (MVDC)	Effective power distribution	Higher cost	PSCAD/ EMTDC-based electromagnetic transient simulations
Baloch et al. (2021)	AdaBoost classifier-based logistic regression (ACLR)	Low cost	Overfitting	MATLAB/Simulink
Baloch et al. (2021)	Data mining	Noise reduction	Overfitting	MATLAB/Simulink
Yan et al. (2020)	Generative adversarial networks (GAN)	Improved generalisation	Long-term stability issues	Not mentioned

The current literature exhibits several drawbacks, including increased expenses, elevated computational complexity, overfitting, stability concerns, and communication overhead. The issues are addressed by applying a hybrid ANN and bidirectional gated recurrent unit (BiGRU).

3 Proposed methodology

The DERs and local loads in the power system can be effectively integrated through the utilisation of the DC-MG mechanism. The incorporation of several sources has the potential to induce instability and faults within MGs. Fault detection are critical for maintaining the stability of the MG system since it allows the protective mechanism to be aware of potential issues. To improve MG dependability, it is critical to use error detection and identification techniques. This work utilises solar and wind as input sources. The extra energy generated by these sources is stored in a battery. Various forms of faults are implemented in the DC-MG. The signals generated by each fault are captured and then analysed using the DWT. The defect in the system is classified using a hybrid ANN and BiGRU after analysing the system condition. The suggested classifier integrates the advantages of both ANN and BiGRU to improve the accuracy of detection. The OOA is employed to optimise the weight parameters of the classifier method in order to minimise iterative errors. Figure 1 illustrates the architecture of the proposed technique.

Figure 1 Architecture of the proposed scheme (see online version for colours)

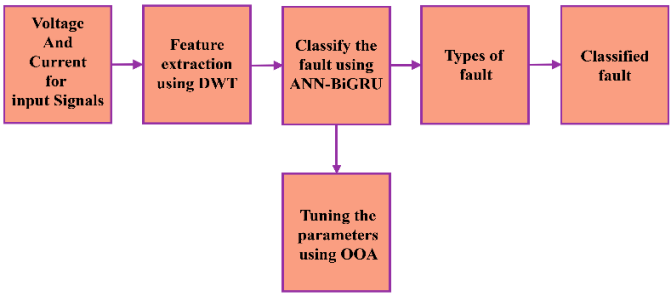

3.1 DWT-based feature extraction

The DWT is employed for feature extraction due to its ability to capture both time and frequency domain information. This makes it particularly suitable for transient signal analysis, which is essential for detecting faults in DC-MGs where voltage and current signals fluctuate dynamically. In the context of a MG, a multitude of problems might arise from several sources, such as external disturbances, lightning strikes, and device malfunctions. Voltage and current are commonly employed as input signals to convey crucial information. The DWT is employed to extract characteristics from voltage and current signals. The DWT is a highly efficient technique for processing time-frequency signals. It allows for precise sampling of signals with temporary characteristics and produces signal restoration that is not duplicated (Veerasamy et al., 2020). Additionally, it facilitates improved localisation of spectral and spatial signals. The DWT tool has been utilised in recent decades for the design of protective relays. The fault current signals $y(\tau)$ are decomposed to lower and higher frequency components, namely detailed coefficients (Z) and approximation (A), as illustrated in equations (1)–(6).

$$y(\tau) = \sum_{\kappa} A_0 \mu_{k,l}(\tau) \tag{1}$$

$$y(\tau) = \sum_{\kappa} A_1 \mu_{k-1,l}(\tau) + \sum_{\kappa} Z_1 \mu_{k-1,l}(\tau) \tag{2}$$

$$y(\tau) = A_1(\tau) + Z_1(\tau) \tag{3}$$

From the above equations, the scaling function is represented by $\mu_{k,l}(\tau)$, approximate coefficients are denoted by A_1, and detailed coefficients are indicated by Z_1. The coefficients that represent the lower frequency component of the signal are decomposed up to a certain level M. The aforementioned procedure is commonly referred to as the decomposition level, which is employed to extract the original information signals from noise. It is mathematically represented as;

$$y(\tau) = A_2(\tau) + Z_2(\tau) + Z_1(\tau) \tag{4}$$

$$y(\tau) = A_3(\tau) + Z_3(\tau) + Z_2(\tau) + Z_1(\tau) \tag{5}$$

$$y(\tau) = A_M(\tau) + Z_M(\tau) + Z_{M-1}(\tau) + \ldots + Z_1(\tau) \tag{6}$$

From the above equations, the decomposition level is represented by M, which allows the optimal decomposition by Γ levels.

$$M = 2^{\Gamma} \tag{7}$$

The method of signal decomposition involves the separation of fault current signals into distinct frequency bands at each level.

$$B = \frac{P}{2^{M+2}} \tag{8}$$

The equation above represents the sampling frequency as P and bandwidth indicated by B.

In the feature extraction phase, the input voltage and current signals are decomposed into various frequency sub-bands using DWT. The DWT divides the signals into approximate and detailed coefficients across multiple levels. These coefficients are then analysed to extract meaningful features that represent changes in signal behaviour during faults. The extracted features serve as inputs to the hybrid ANN-BiGRU model for further classification.

3.2 Proposed hybrid ANN-BiGRU architecture-based classification

The features obtained from the DWT are utilised in the hybrid ANN-BiGRU model to categorise and detect problems in the MG system. The present study introduces a hybrid model that integrates two neural network designs, namely ANN and BiGRU. The primary goal of the suggested methodology is to enhance the precision of defect identification. In a conventional ANN, each hidden layer, including the input and output layers, contributes to feature extraction. Feature extraction in ANNs occurs mostly in the hidden layers. The BiGRU unit is a computational model based on a bidirectional RNN. It consists of two layers of GRUs that transmit information in different directions. To enhance the utilisation of input information, the BiGRU configuration integrates a reverse layer into the single-layer GRU network. This architectural design utilises two concealed layers to record historical and prospective data. ANNs encounter challenges such as overfitting

when presented with data of larger dimensionality. BiGRU networks have demonstrated a good handling of time series and higher dimensional data because of their unique structure. However, it is worth mentioning that these networks may struggle to capture the data's features explicitly at times. The construction of the hybrid ANN-BiGRU is illustrated in Figure 2.

Figure 2 Structure of hybrid ANN-BiGRU (see online version for colours)

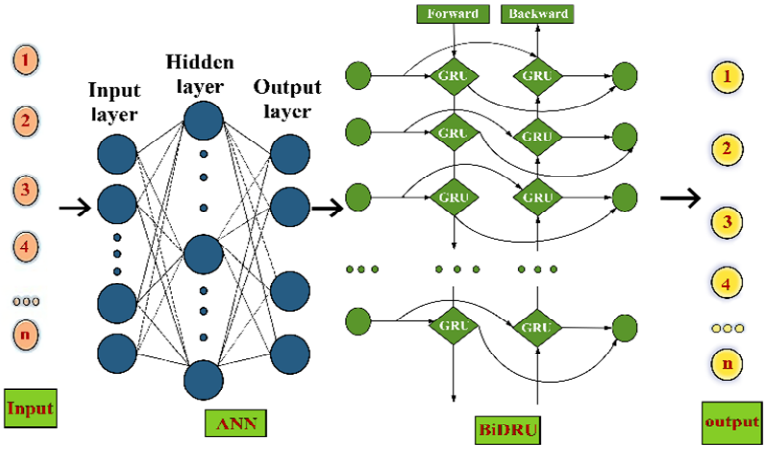

In comparison to BiGRU, ANN with BiGRU offers improved test accuracy with nearly equal weights and a shorter training period. As a result, ANN enables quicker training, cutting down on the amount of time needed for huge data. Additionally, the ANN-BiGRU classifiers have multiple layers to extract the intricate characteristics from the datasets. An output layer extracts BiGRU features and a predetermined number of hidden layers from the ANN, while an input layer receives the parameters as input.

3.3 Osprey optimisation algorithm

The OOA is used to decrease the inaccuracy when tuning the weight values. The OOA algorithm is classified as a bio-inspired metaheuristic algorithm. The optimisation technique is designed based on the eating and hunting behaviours of ospreys. The main steps of the OOA algorithm are initialisation, exploitation and exploration. The ospreys mathematical model is employed to enhance the OOA (Ismaeel et al., 2023; Somula et al., 2024).

3.3.1 Initialisation

The OOA is a population-based approach used to iteratively explore a problem-solving space to identify the optimal solution. In the population, each individual is considered to adjust the weight parameters represented by equation (9).

$$P = \begin{bmatrix} P_1 \\ \vdots \\ P_j \\ \vdots \\ P_o \end{bmatrix}_{o\times n} = \begin{bmatrix} p_{1,1} & \cdots & p_{1,k} & \cdots & p_{1,n} \\ \vdots & \ddots & \vdots & \ddots & \vdots \\ & \cdots & p_{j,k} & \cdots & p_{j,n} \\ \vdots & \ddots & \vdots & \ddots & \vdots \\ & \cdots & p_{o,k} & \cdots & p_{o,n} \end{bmatrix}_{o\times n} \tag{9}$$

The network comprises O number of faults, which are randomly initialised using the below equation.

$$P_{j,k} = mpc_k + s_{j,k}\left(vqc_k - mpc_k\right) \quad j = 1, 2, \ldots, o \; k = 1, 2, \ldots, n \tag{10}$$

The main objective of this algorithm is to tune the fitness weight parameter by finding the minimum error.

From the above equation, the population matrix of the ospreys is denoted by P, the k^{th} osprey is denoted by P_j, and k^{th} dimension of the j^{th} osprey is represented by $P_{j,k}$, the number of the ospreys is represented by o, and the count of problem variables is denoted by n. The random values among 1 and 0 are represented by $s_{j,k}$, the lower bound and the upper bound is indicated by mpc_k and vqc_k.

$$E = \begin{bmatrix} E_1 \\ \vdots \\ E_j \\ \vdots \\ E_o \end{bmatrix}_{o\times 1} = \begin{bmatrix} E(P_1) \\ \vdots \\ E(P_j) \\ \vdots \\ E(P_o) \end{bmatrix}_{o\times 1} \tag{11}$$

The values of the objective function are indicated by E and E_j indicates the value of the objective function corresponding to j^{th} osprey. The estimated values are utilised to assess the quantity of the candidate's responses. The iterative procedure involves selecting the most optimum and least ideal members by considering the worst and best values. Each iteration involves updating and evaluating the position of the ospreys.

3.3.2 Phase 1: exploration

By locating the undersea fish in the water, ospreys use their acute vision to seek and locate prey. After locating the fish, the osprey attacks by diving into the water to get its prey. In the early stages of the OOA, the position is updated using a model derived from osprey behaviour. The group of fish targeted by each osprey is determined by equation (12).

$$E_{Ps_j} = \left\{P_\chi \,\middle|\, \chi \in \{1, 2, \ldots, m\} \wedge EI_\chi < EI_j\right\} \cup \left\{P_{BST}\right\} \tag{12}$$

The group of the fish for j^{th} osprey is represented by E_{Ps_j}, P_{BST} indicates the best osprey. Ospreys attack the submerged fish in an attempt to determine its position at random. The osprey's movement toward the fish in search space indicates its new location. Replace the osprey's last position with equation (13) if the modified position produces a greater objective value than the prior one.

$$p_{j,k}^{Ps1} = p_{j,k} + \Re AN_{j,k} \cdot \left(\delta f_{j,k} - \Re_{j,k} \cdot z_{j,k}\right) = \begin{cases} p_{j,k}^{Ps1}, & mpc_k \le p_{j,k}^{Ps1} \le vqc_k; \\ mpc_k, & p_{j,k}^{Ps1} < mpc_k; \\ vqc_k, & p_{j,k}^{Ps1} > vqc_k; \end{cases} \tag{13}$$

$$P_j = \begin{cases} P_j^{Ps1}, & EI_j^{Ps1} < EI_j; \\ P_j, & \text{else} \end{cases} \tag{14}$$

The new position of j^{th} osprey with the initial phase of OOA is represented by P_j^{Ps1}, $\delta f_{j,k}$ is denoted as fish selected for i^{th} osprey, k^{th} dimension is represented by $P_{j,k}^{Ps1}$, the value of the objective function is indicated by EI_j^{Ps1}, and $\Re AN_{j,k}$ indicates the random interval [0, 1] as well as $\Re_{j,k}$ indicates the random number [1, 2].

Figure 3 Flow diagram of OOA (see online version for colours)

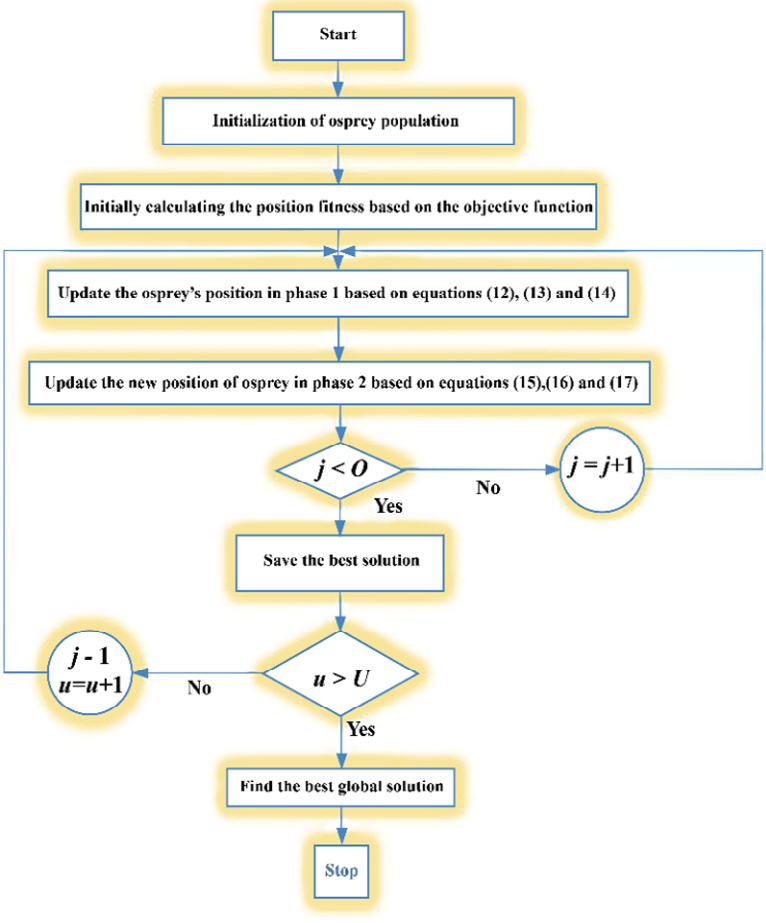

3.3.3 Phase 2: exploitation

The osprey is the safest location to consume the fish after hunting. The purpose of the second stage of OOA is to update the population based on osprey behaviour. During the OOA design phase, osprey behaviour is simulated to determine the population's random position for consuming the hunted fish, as shown in equation (15).

$$p_{j,k}^{Ps2} = p_{j,k} + \frac{mpc_k + \Re AN_{j,k} \cdot (vqc_k - LOW_k)}{l}, \quad j = 1, 2, 3, \ldots, o, k = 1, 2, \ldots, n, l = 1, 2, \ldots, u \tag{15}$$

$$y_{j,k}^{Ps2} = \begin{cases} p_{j,k}^{Ps2}, & mpc_k \le p_{j,k}^{Ps2} \le vqc_k; \\ mpc_k, & p_{j,k}^{Ps2} < mpc_k; \\ vqc_k, & p_{j,k}^{Ps2} > vqc_k; \end{cases} \tag{16}$$

$$P_j = \begin{cases} P_j^{Ps2}, & EI_j^{Ps2} < EI_j; \\ P_j, & \text{else} \end{cases} \tag{17}$$

The new position of j^{th} osprey with OOA second phase is indicated by P_j^{Ps2}, k^{th} dimension is represented by $P_{j,k}^{Ps2}$, the value of the objective function is indicated by EI_j^{Ps2}, the algorithm iteration counter is represented by l, and the number of iterations is denoted by L. The flow diagram of OOA is depicted in Figure 3.

Figure 4 Test system of DC-MG (see online version for colours)

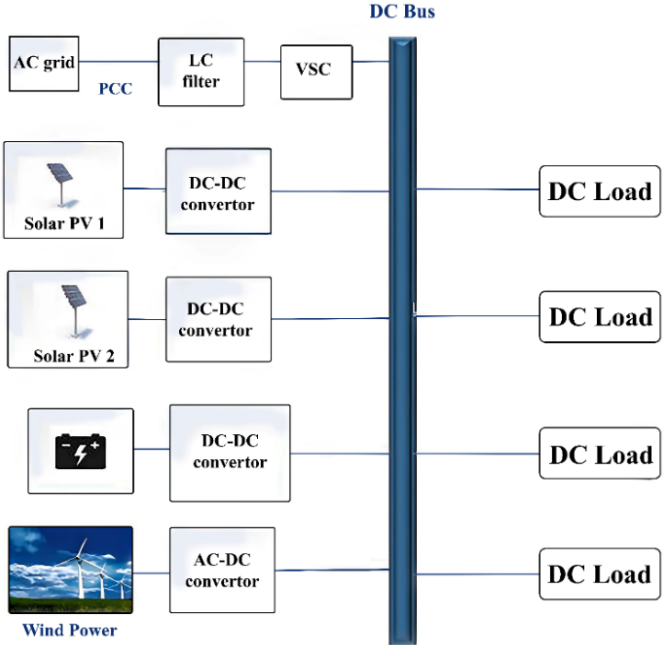

4 Test system

In this section, the DC-MG system is briefly explained. The DC-MG schematic diagram is shown in Figure 4. The distributed generating units are the two solar photovoltaic (SPV) units, the DC loads, and the energy storage systems with batteries (BESS). The DC bus is connected to the main grid via the VSC. It allows power to flow bidirectionally between two grids. Based on the point of common coupling (PCC) connection, the two main working modes are isolated and grid-connected. In DC-MGs, the supercapacitor and battery are the two common energy storage devices used. Connected to the DC bus, the wind and solar PV systems can operate in either maximal power point tracking mode or reduced power mode. A DC-MG that is integrated into a MATLAB/Simulink system is used to validate the suggested approach.

4.1 Dataset generation

Initially, the dataset is generated in the Simulink/MATLAB environment to stimulate different operating conditions on a DC-MG. In a DC-MG, different kinds of faults are applied to generate datasets. No fault, solar line to line fault (LL), wind LL fault, solar line to ground (LG) fault, wind LG fault, short circuit fault in battery (SCF), convertor fault (CF), DC capacitor fault (DF), solar pole to pole (PP) fault, wind PP fault, positive pole to ground (PPG), negative pole to ground (NPG), series arc fault (SAF), shunt arc fault (ShAF), cable faults (C1F), removing load (RL), and increasing load (RL) are some common types of fault applied in DC-MG that are commonly encountered.

5 Simulation results

A variety of parameters are used to validate and verify performance. Recall, precision, and accuracy are the three statistical measures used to analyse the proposed hybrid ANN-BiGRU model's performance. The parameters' performance is described and stated as follows;

- *Accuracy:* It calculates the consistency between predicted and actual events encompassing both fault events and non-fault events. It is expressed as:

$$\frac{\tau o \tau\left(\hat{E}+\hat{\bar{E}}\right)}{\tau o \tau\left(E+\bar{E}\right)} \tag{18}$$

  From the above equation, $\hat{E}$ indicates the predicted faults and $\hat{\bar{E}}$ denotes the no-fault events, although no-fault and actual fault events are represented by $\bar{E}$ and E.

- *Precision:* The statistic parameter is crucial for precisely establishing the relationship between actual and predicted occurrences in order to evaluate the reliability of fault detection. Subsequently, it is articulated as:

$$\frac{\tau o \tau\ \hat{E}}{\tau o \tau\ E} \tag{19}$$

- *Recall:* It illustrates the overall number of events that are no-fault but are identified as fault events, and it is calculated as:

$$\frac{\tau o \tau \hat{\bar{E}}}{\tau o \tau \bar{\bar{E}}} \tag{20}$$

Figure 5 P-V and I-V characteristics of solar PV are based on, (a) normal operation (b) faulty conditions (see online version for colours)

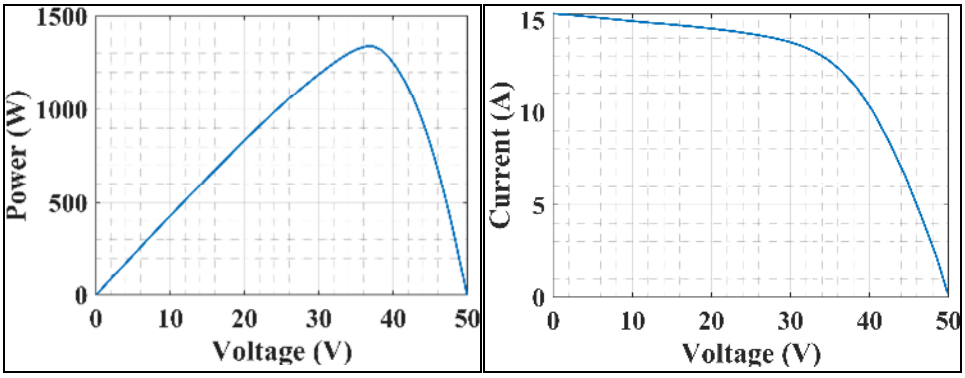

(a)

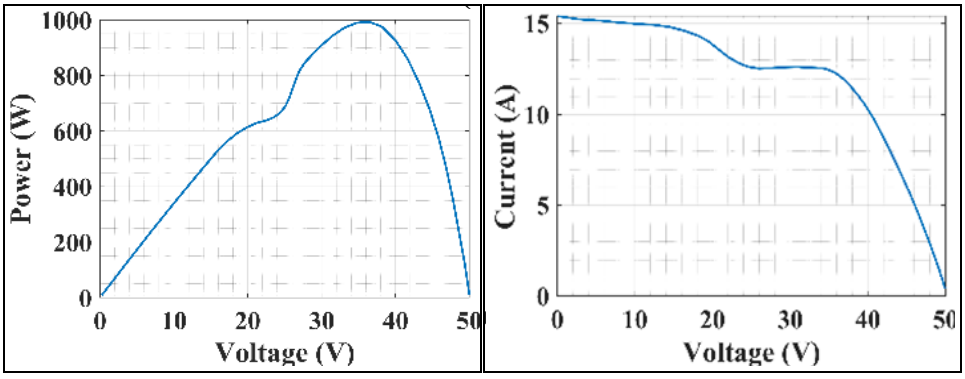

(b)

Figure 5 depicts the P-V and I-V characteristics of solar PV systems. Before the occurrence of the issue, the maximum power point was seen to be 1,300 W, while the estimated open circuit voltage was 50 V. When faults are present, there is a deviation from the original shapes of both the maximum power point and current waveforms.

The faulty output of solar PV is illustrated in Figure 6. The solar PV system is interconnected through DC-DC power converters, and any malfunctions occurring within the PV system are commonly attributed to the presence of short circuit currents. In partial shade conditions, both the temperature and open circuit voltage exhibit a rise. LL faults develop within the wires of a PV array. Ground faults may occasionally manifest within the solar PV modules. The LL fault is delivered at intervals of 0.5 seconds, resulting in waveform distortion. Under defective conditions, the voltage drops, and the current deviates from the solar PV system's nominal values.

Figure 6 Solar output with faulty resistance of 0.5Ω (see online version for colours)

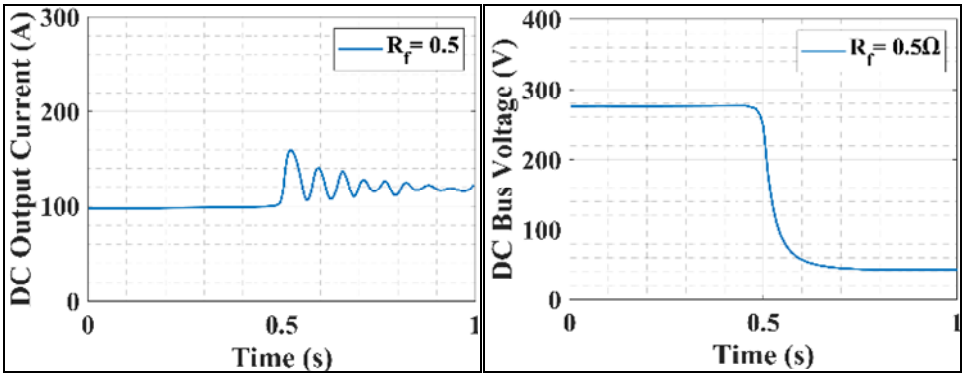

(a) (b)

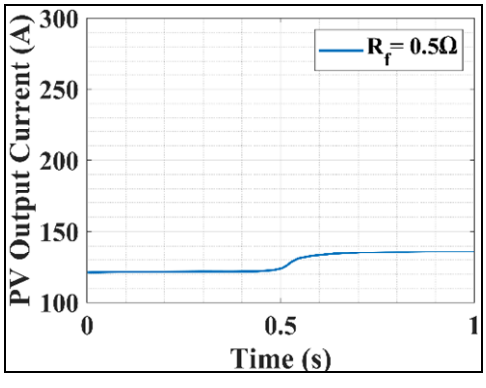

(c)

Figure 7 illustrates the occurrence of the LG fault at regular intervals of 0.5 seconds in the solar PV system. Upon the occurrence of a defect, the voltage, power, and current of the array are reduced to 11.5 V, 1,400 W, and 155 A, respectively.

Figure 7 Solar PV output with LG fault (see online version for colours)

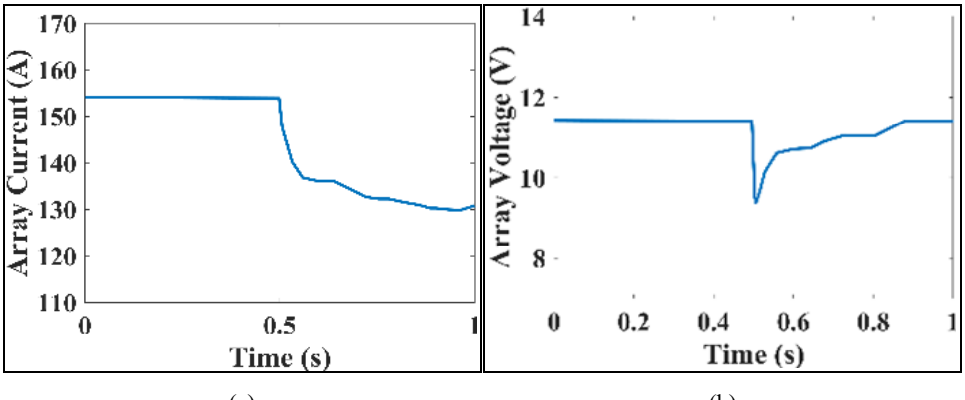

(a) (b)

Figure 7 Solar PV output with LG fault (continued) (see online version for colours)

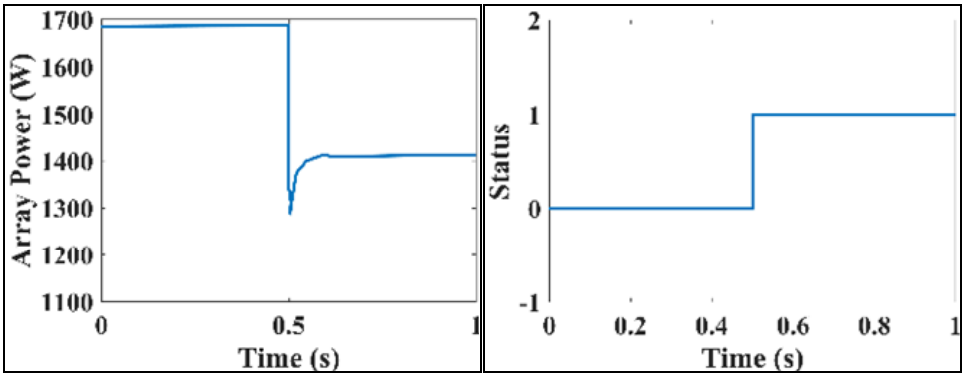

(c) (d)

Figure 8 Solar output with LL fault (see online version for colours)

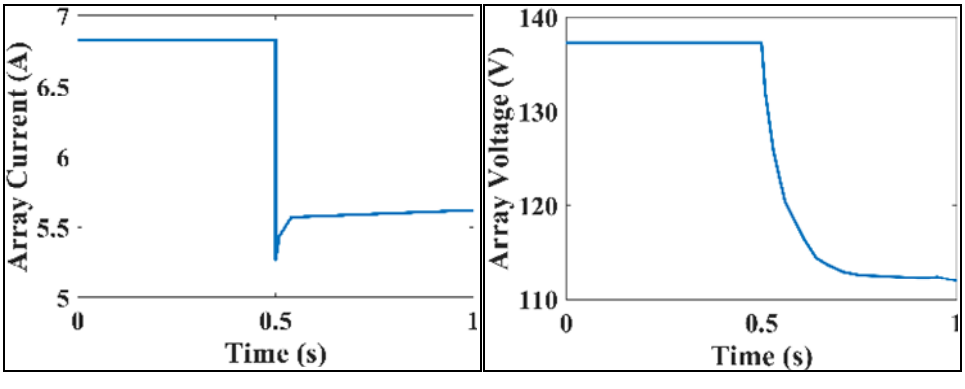

(a) (b)

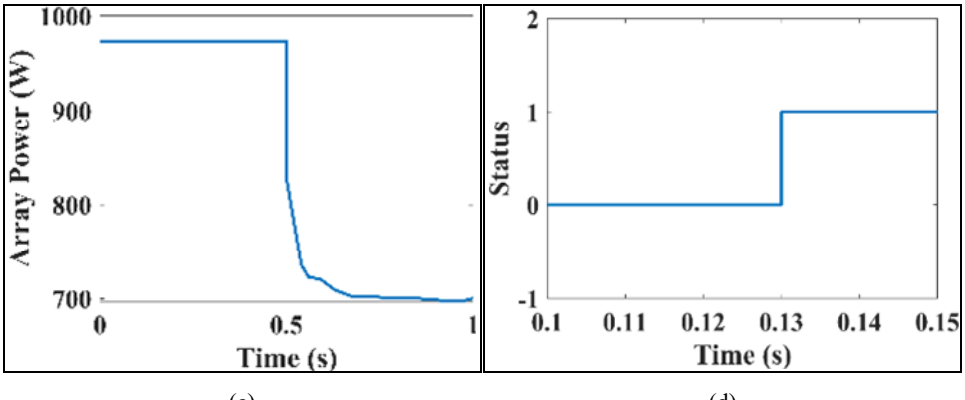

(c) (d)

Figure 9 Applying faults in the battery (a) current (b) DC bus voltage (see online version for colours)

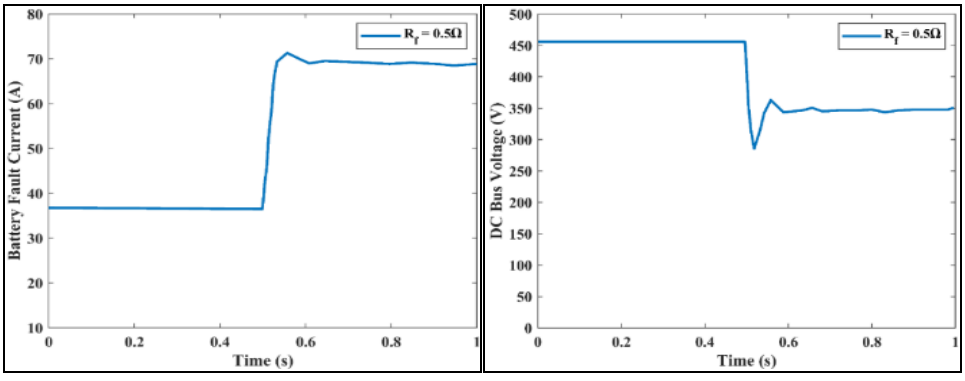

(a) (b)

Figure 10 PP fault waveforms, (a) DC bus voltage (b) solar PV current (see online version for colours)

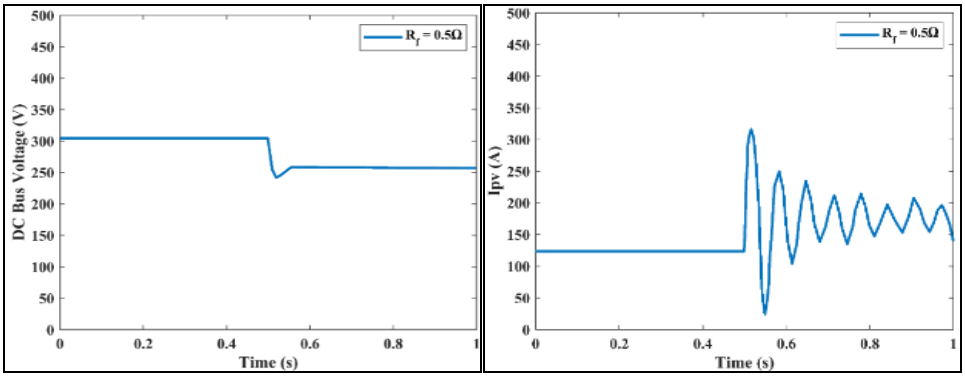

(a) (b)

Figure 11 Waveforms based on PG fault (see online version for colours)

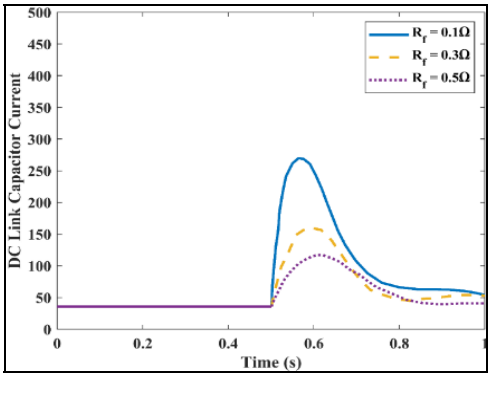

Figure 12 Waveforms of current and voltage with fault resistance, (a) 0.1Ω (b) 2Ω (c) 100Ω (see online version for colours)

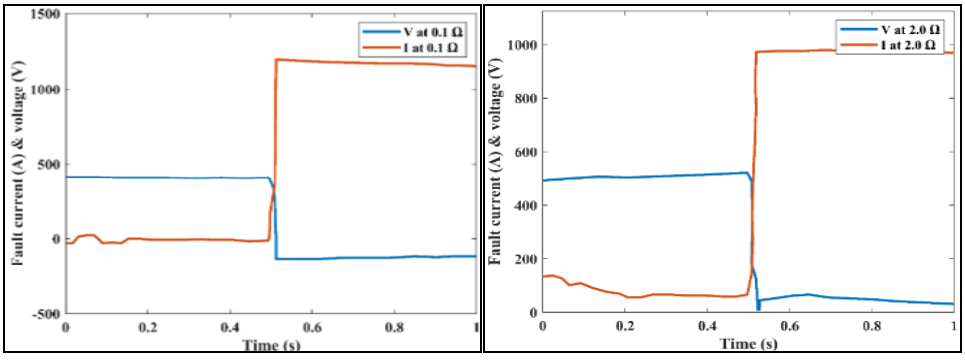

(a) (b)

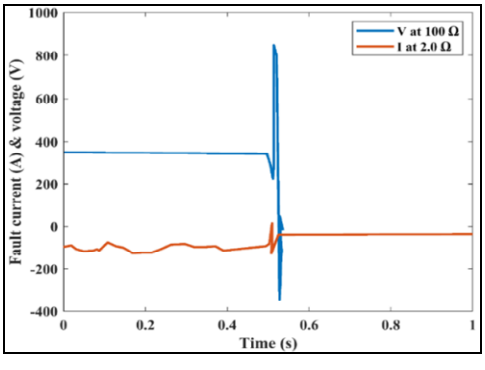

(c)

The LL fault is triggered at regular intervals of 0.5 seconds in the solar PV system, and the resulting outcomes are illustrated in Figure 8. When an LL fault occurs, it leads to a decrease in voltage, current, and power values.

Figure 13 Wind current, (a) LG fault (b) LL fault (c) PP fault (see online version for colours)

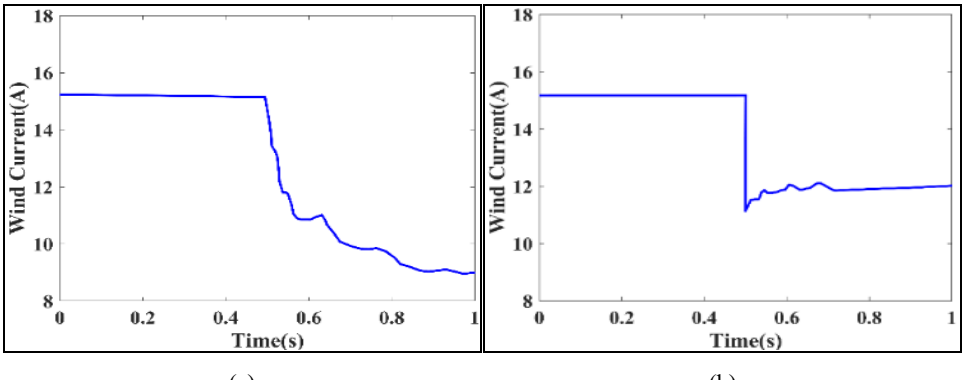

(a) (b)

Figure 13 Wind current, (a) LG fault (b) LL fault (c) PP fault (continued) (see online version for colours)

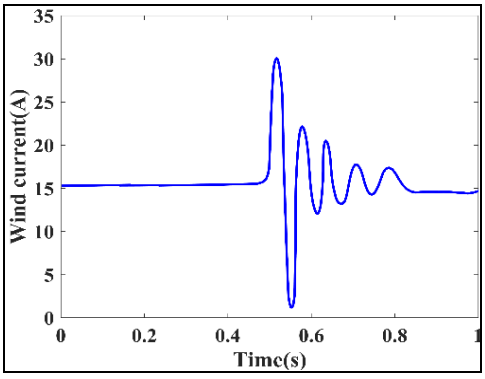

(c)

Figure 14 Wind power, (a) LG fault (b) LL fault (see online version for colours)

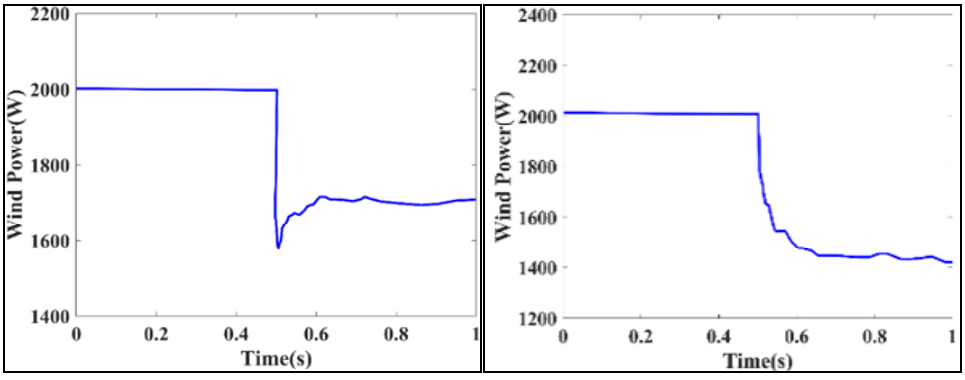

(a) (b)

Figure 9 depicts the estimated current at the battery terminal resulting from the faulty process. Creating a short circuit in the battery might result in significant electrical shocks throughout the system. During the issue, the battery current exceeds the normal value while the voltage decreases.

The PP failure waveforms in the DC bus system are depicted in Figure 10. During faulty, the electrical current in both the battery and solar PV systems is reduced, as observed earlier. The waveforms are assessed in these defective conditions, with a faulty resistance of 0.5 Ω.

The waveforms of the DC link capacitor output, shown in Figure 11, indicate a PG fault. The results suggest that the current flowing through the capacitor exhibits oscillations when subjected to a failure state. Furthermore, it is observed that the DC link voltage exhibits a fall below its nominal value when subjected to varying fault situations.

Figure 12 illustrates the waveforms of current and voltage in the presence of fault resistance. The results are verified by multiple degrees of fault resistance. During a fault condition, there is an increase in bus current and a drop in bus voltages. The augmentation of fault resistance leads to an elevation in the peak value of fault current.

Figure 15 Wind voltage, (a) LG fault (b) LL fault (see online version for colours)

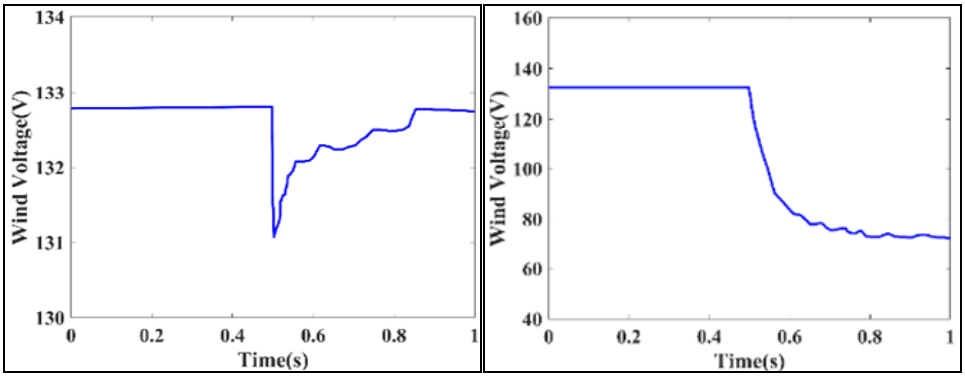

(a) (b)

Figure 16 Current flow by cable (a) PP (b) PPG (c) NPG (see online version for colours)

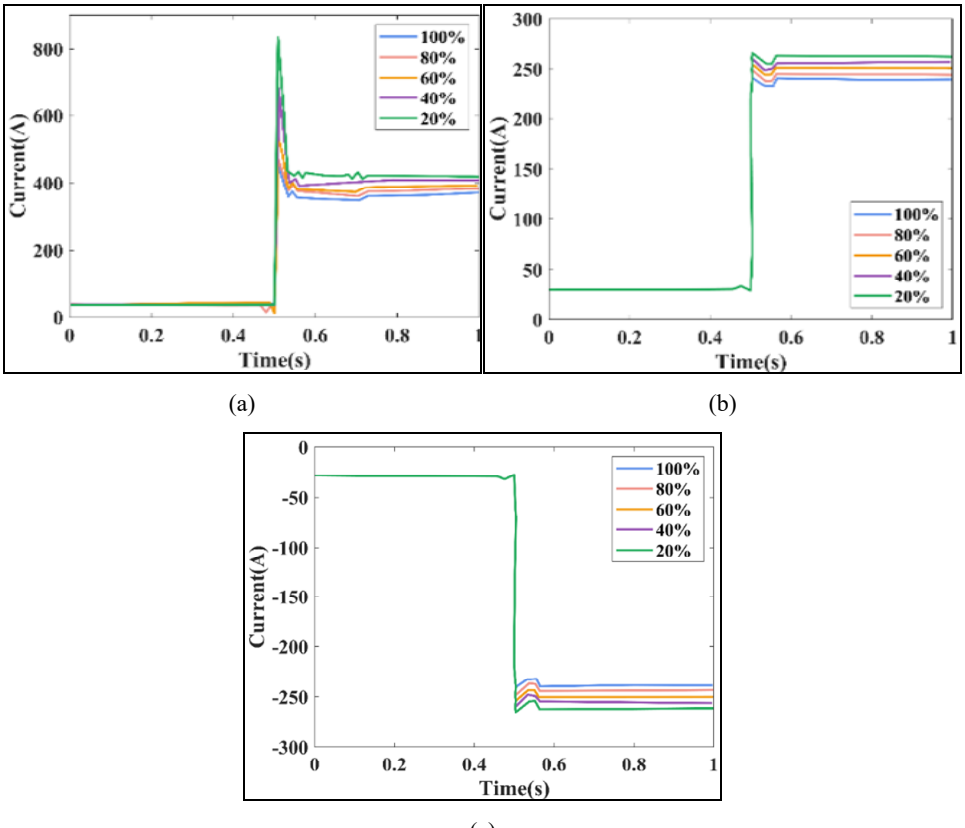

(a) (b)

(c)

Figure 13 illustrates the occurrence of the LG fault, LL fault, and PP fault in the Wind current. Every 0.5 seconds, the LG, LL, and PP faults are imposed. When the LG fault is applied, the wind current is reduced. During an LL fault, the wind current diminishes

before attaining a state of stability. In the event of a PowerPoint fault, the wind current undergoes fluctuations, resulting in a stable value after a duration of 0.8 seconds.

The LG and LL faults seen in wind power are depicted in Figure 14. In the event of an LG fault, there is an initial reduction in wind output, followed by a subsequent minor increase. During the application of an LL fault, the wind power is reduced, and it will reach a steady value.

Figure 17 Current flow by cable, (a) series arc fault and (b) shunt arc fault (see online version for colours)

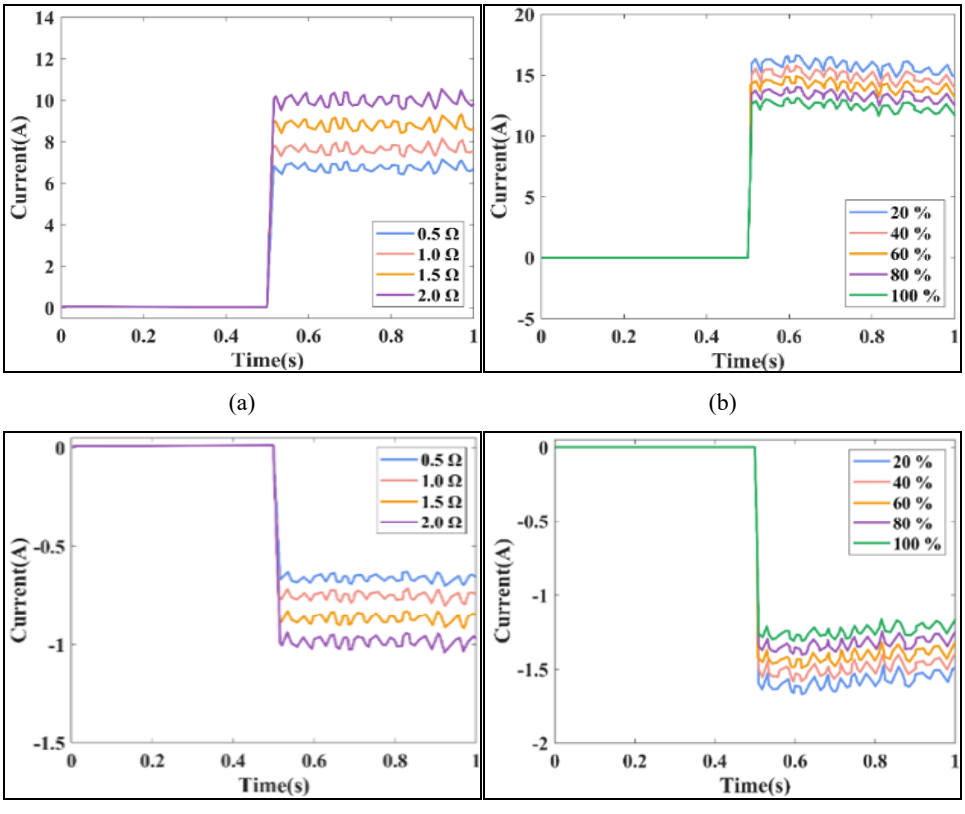

The occurrences of LG and LL faults in wind power systems are illustrated in Figure 15. During the implementation of the LG fault, there is an initial fall in wind voltage followed by subsequent increases. In the event of an LL fault, the wind voltage is reduced and then returns to a stable state.

The proposed defect detection method performs better under these circumstances. The PP, PPG, and NPG faults that can develop in transmission lines are shown in Figure 16. There are faults applied every 0.5 seconds. When the fault distance increases in the PP scenario, the current peak value initially decreases. The initial peak value observed during a fault situation is lower for PPP faults than for PP faults. In the NPG situation, the initial negative peak value increases as the fault distance decreases.

Figure 18 Training and testing accuracy and loss of the proposed technique (see online version for colours)

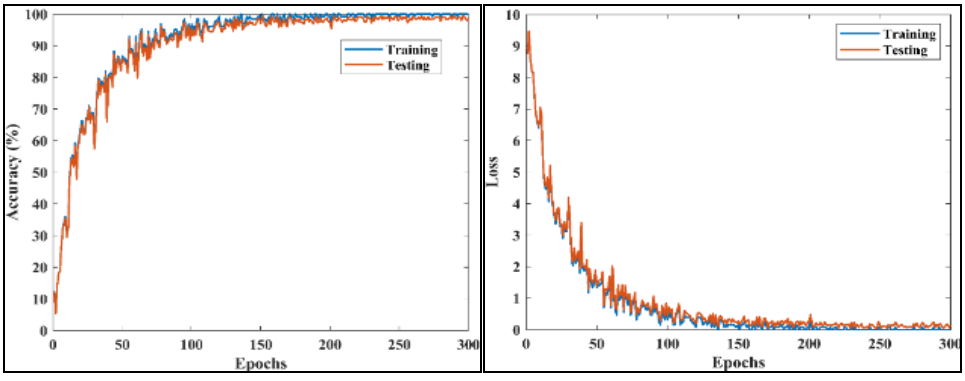

(a) (b)

Figure 19 Confusion matrix

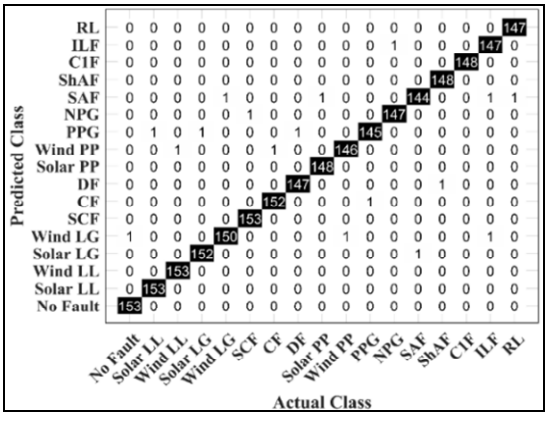

The DC-MG's shunt and series arc faults are depicted in Figure 17. The peak current value in ShAF falls as the fault resistance value rises. The fault in a series arc decreases as resistance rises.

Figure 18 presents the accuracy and loss of the proposed method across epochs. The proposed technique has enhanced accuracy by 99.65% with a loss of 0.35. Figure 19 illustrates the confusion matrix of the proposed technique for 17 classes. The figure indicates that most classes are classified accurately, with few misclassified samples.

Figure 20 depicts the convergence plot of OOA with other optimisation algorithms, such as the Ebola optimisation algorithm (EOA), particle swarm optimisation (PSO), and the whale optimisation algorithm (WOA). The optimisation technique aims to minimise the error of ANN-BiGRU. Therefore, it is formulated as a minimisation problem. Using OOA, the minimum fitness is achieved by the 18th iteration. Existing optimisations like EOA, PSO, and WOA require more iterations of 70, 58, and 38, respectively.

Figure 20 Convergence of OOA with other conventional optimisation (see online version for colours)

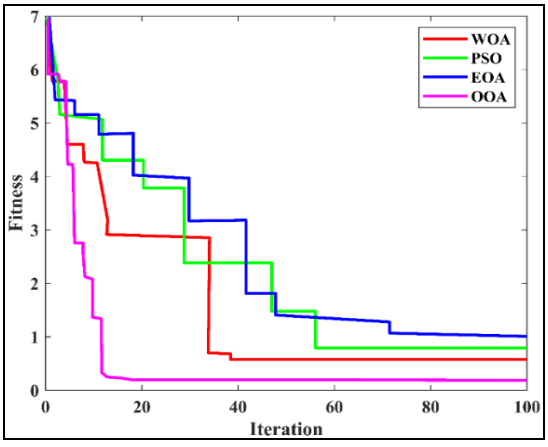

Figure 21 Comparative analysis of performance (see online version for colours)

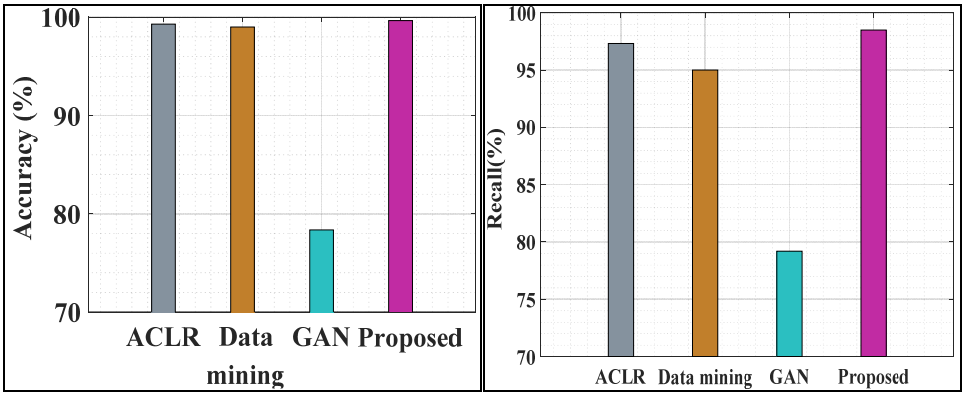

(a) (b)

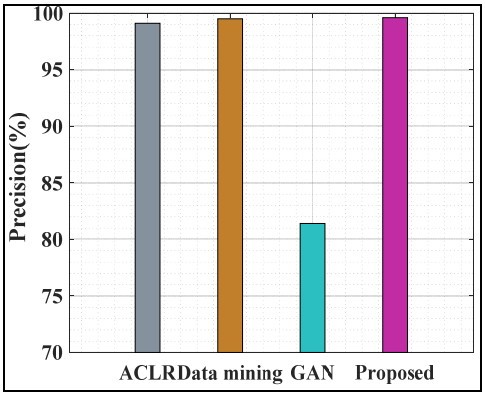

(c)

Figure 22 Comparative analysis of the proposed technique with other existing methods (see online version for colours)

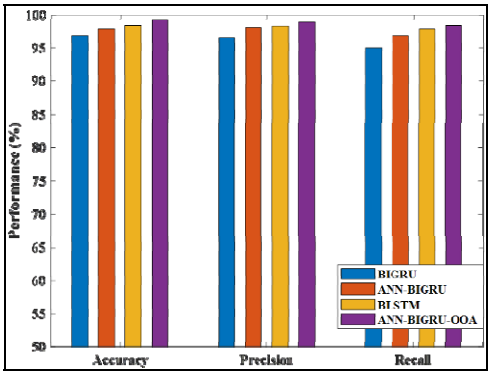

Figure 23 Comparison of the overall error (see online version for colours)

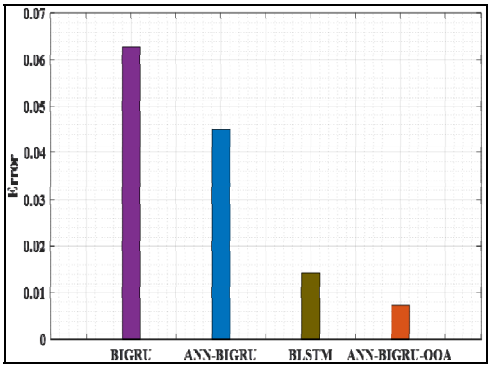

Figure 24 Comparison of detection time (see online version for colours)

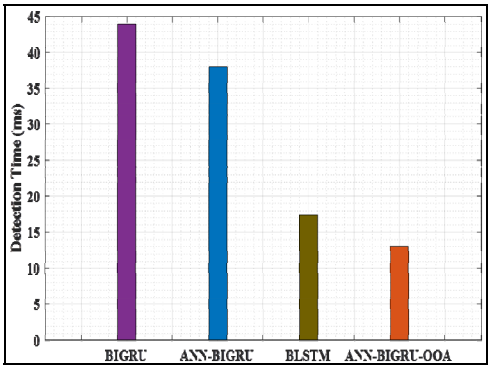

Figure 21 illustrates the comparative analysis of performance. The proposed hybrid ANN-BiGRU is compared with other state-of-art methods such as ACLR, data mining, and GAN. The proposed technique acquired higher accuracy, precision, and recall of 99.65%, 99.60%, and 98.5%.

Figure 22 depicts the performance comparison of the proposed technique with other existing methods, analysing accuracy, precision, and recall as performance measures. When compared to other existing techniques, the proposed technique acquired a higher accuracy of 99.65%, precision of 99.60%, and recall of 98.5%.

The error acquired from the detection process is illustrated in Figure 23. The proposed technique obtains less error than other existing techniques. Figure 24 depicts the comparison of detection time. The existing methods, including ANN, ANN-BiGRU, and BLSTM, are utilised to compare with the proposed approach. The detection time for the existing approaches is very high, with the ranges of 54 s and 48 s. Therefore, the proposed technique is fast and detects faults in 13 s.

5.1 Discussion

This work utilises the proposed hybrid ANN-BiGRU technique for the identification and categorisation of faults. This section presents an analysis of the proposed technique in comparison with existing techniques. The proposed technique is compared with existing techniques like ANN, ANN-BiGRU, and BLSTM. Low performance, higher detection time, and higher error are major problems with the existing methods. The ANN-BiGRU-OOA technique is proposed to address these difficulties. The proposed technique outperformed the current methods in terms of performance, error rate, and fault detection time. Fine-tuning parameters and selecting relevant features improve the efficiency of the proposed technique, enabling faster fault detection.

Table 2 Performance analysis

Technique	*Accuracy*	*Precision*	*Recall*
ACLR	99.29%	99.1%	97.33%
Data mining	99%	99.5%	95%
GAN	78.36%	81.4%	79.2%
Proposed hybrid ANN-BiGRU	99.65%	99.60%	98.5%

Table 2 illustrates the performance analysis of existing techniques with the proposed approach.

6 Conclusions

This paper presents a hybrid ANN-BiGRU technique for detecting and classifying faults based on the DC-MG. By effectively extracting features from voltage and current signals using DWT and the features being classified using hybrid ANN-BiGRU, the approach achieves a significant improvement in performance compared to existing techniques. In this paper, MATLAB/Simulink is utilised to design the simulation of a DC-MG. Parameters like accuracy, precision, and recall are computed for the proposed approach compared to existing approaches. The comparative analysis demonstrated higher accuracy for the proposed hybrid ANN-BiGRU approach. The proposed hybrid ANN-BiGRU obtained 99.65% accuracy, 99.60% precision, and 98.5% recall. This performance evaluation indicates the performance of the proposed approach for identifying and classifying the faults in the DC-MG system. However, the hybrid

ANN-BiGRU model may be computationally complex, potentially limiting its applicability in real-time applications. In addition, future research will use less computationally complex methods to improve the security, dependability, and effectiveness of protection systems against power supply faults while considering various configuration modes of the MG.

References

Abdelsalam, A.A. (2020) 'Optimal distributed energy resources allocation for enriching reliability and economic benefits using sine-cosine algorithm', *Technology and Economics of Smart Grids and Sustainable Energy*, Vol. 5, pp.1–18.

Alhanaf, A.S., Farsadi, M. and Balik, H.H. (2024) 'Fault detection and classification in ring power system with DG penetration using hybrid CNN-LSTM', *IEEE Access*, Vol. 12, pp.59953–59975.

Ali, Z., Terriche, Y., Abbas, S.Z., Hassan, M.A., Sadiq, M., Su, C.L. and Guerrero, J.M. (2021) 'Fault management in DC microgrids: a review of challenges, countermeasures, and future research trends', *IEEE Access*, Vol. 9, pp.128032–128054.

Baloch, S. and Muhammad, M.S. (2021) 'An intelligent data mining-based fault detection and classification strategy for microgrid', *IEEE Access*, Vol. 9, pp.22470–22479.

Baloch, S., Samsani, S.S. and Muhammad, M.S. (2021) 'Fault protection in microgrid using wavelet multiresolution analysis and data mining', *IEEE Access*, Vol. 9, pp.86382–86391.

Barik, S.K. (2023) 'Fault detection and classification of DC microgrid based on VMD', *COMPEL – The International Journal for Computation and Mathematics in Electrical and Electronic Engineering*, Vol. 42, No. 2, pp.302–322.

Bayati, N., Baghaee, H.R., Hajizadeh, A., Soltani, M. and Lin, Z. (2021a) 'Mathematical morphology-based local fault detection in DC microgrid clusters', *Electric Power Systems Research*, Vol. 192, p.106981.

Bayati, N., Baghaee, H.R., Hajizadeh, A., Soltani, M., Lin, Z. and Savaghebi, M. (2021b) 'Local fault location in meshed DC microgrids based on parameter estimation technique', *IEEE Systems Journal*, Vol. 16, No. 1, pp.1606–1615.

Cepeda, C., Orozco-Henao, C., Percybrooks, W., Pulgarín-Rivera, J.D., Montoya, O.D., Gil-González, W. and Vélez, J.C. (2020) 'Intelligent fault detection system for microgrids', *Energies*, Vol. 13, No. 5, p.1223.

Chandra, A., Singh, G.K. and Pant, V. (2020) 'Protection techniques for DC microgrid – a review', *Electric Power Systems Research*, Vol. 187, p.106439.

Chandra, M.S.S. and Mohapatro, S. (2023) 'Hybrid sensor fault tolerant control of low voltage DC microgrid', *IEEE Transactions on Industry Applications*, Vol. 60, No. 1, pp.1705–1715.

Chowdhury, M.R., Jobayer, A.M. and Zhao, L. (2021) 'Potential of distributed energy resources for electric cooperatives in the united states', in *2021 IEEE/IAS 57th Industrial and Commercial Power Systems Technical Conference (I&CPS)*, IEEE, pp.1–9.

Das, S.K., Namasudra, S. and Sangaiah, A.K. (2024) 'HCNNet: hybrid convolution neural network for automatic identification of ischaemia in diabetic foot ulcer wounds', *Multimedia Systems*, Vol. 30, No. 1, p.36.

Deotti, L., Silva Jr., I., Honório, L. and Marcato, A. (2021) 'Empirical models applied to distributed energy resources – an analysis in the light of regulatory aspects', *Energies*, Vol. 14, No. 2, p.326.

Gajula, K., Le, V., Yao, X., Zou, S. and Herrera, L. (2023) 'A probabilistic approach to series arc fault detection and identification in DC microgrids', *IEEE Journal of Emerging and Selected Topics in Industrial Electronics*, Vol. 5, No. 1, pp.27–38.

Grcić, I., Pandžić, H. and Novosel, D. (2021) 'Fault detection in dc microgrids using short-time Fourier transform', *Energies*, Vol. 14, No. 2, p.277.

Irfan, M.M., Supriya, R., Reddy, P.M., Alabdeli, H. and Gurumoorthy, S. (2024) 'Bi-directional gated recurrent unit approach for detecting and classifying high impedance fault in power distribution', in *2024 Third International Conference on Distributed Computing and Electrical Circuits and Electronics (ICDCECE)*, IEEE, pp.1–5.

Ismaeel, A.A., Houssein, E.H., Khafaga, D.S., Abdullah Aldakheel, E., AbdElrazek, A.S. and Said, M. (2023) 'Performance of osprey optimization algorithm for solving economic load dispatch problem', *Mathematics*, Vol. 11, No. 19, p.4107.

Jadidi, S., Badihi, H. and Zhang, Y. (2020) 'Fault diagnosis in microgrids with integration of solar photovoltaic systems: a review', *IFAC-PapersOnLine*, Vol. 53, No. 2, pp.12091–12096.

Khaleefah, S.H., Mostafa, S.A., Gunasekaran, S.S., Khattak, U.F., Yaacob, S.S. and Alanda, A. (2024) 'A deep learning-based fault detection and classification in smart electrical power transmission system', *JOIV: International Journal on Informatics Visualization*, Vol. 8, No. 2, pp.812–818.

Khan, S.S. and Wen, H. (2021) 'A comprehensive review of fault diagnosis and tolerant control in DC-DC converters for DC microgrids', *IEEE Access*, Vol. 9, pp.80100–80127.

Lakshmi, G.S., Rubanenko, O., Divya, G. and Lavanya, V. (2020) 'Distribution energy generation using renewable energy sources', in *2020 IEEE India Council International Subsections Conference (INDISCON)*, IEEE, pp.108–113.

Mao, J., Ye, S., Li, T., Chen, M. and Chen, B. (2024) 'Secure state estimation of DC microgrid system under false data injection attack', *IEEE Access*, Vol. 12, pp.33524–33535.

Modi, S. and Usha, P. (2023) 'Microgrid protection challenges and solution', in *IOP Conference Series: Materials Science and Engineering*, IOP Publishing, Vol. 1295, No. 1, p.012014.

Montoya, R., Poudel, B.P., Bidram, A. and Reno, M.J. (2022) 'DC microgrid fault detection using multiresolution analysis of traveling waves', *International Journal of Electrical Power & Energy Systems*, Vol. 135, p.107590.

Moradmand, A., Dorostian, M. and Shafai, B. (2021) 'Energy scheduling for residential distributed energy resources with uncertainties using model-based predictive control', *International Journal of Electrical Power & Energy Systems*, Vol. 132, p.107074.

Nougain, V., Mishra, S., Nag, S.S. and Lekić, A. (2023) 'Fault location algorithm for multi-terminal radial medium voltage DC microgrid', *IEEE Transactions on Power Delivery*, Vol. 38, No. 6, pp.4476–4488.

Pragati, A., Gadanayak, D.A. and Mishra, M. (2024) 'Fault detection and fault phase identification in a VSC-MT-HVDC link using Stockwell transform and Teager energy operator', *Electric Power Systems Research*, Vol. 236, p.110937.

Salehimehr, S., Miraftabzadeh, S.M. and Brenna, M. (2024) 'A novel machine learning-based approach for fault detection and location in low-voltage DC microgrids', *Sustainability*, Vol. 16, No. 7, p.2821.

Sasaki, K., Aki, H. and Ikegami, T. (2022) 'Application of model predictive control to grid flexibility provision by distributed energy resources in residential dwellings under uncertainty', *Energy*, Vol. 239, p.122183.

Saurabh, P., Velmurugan, K., N, N., Patange, G., Mohan Raj, G.B., Amarendra, C. and Kumar Reddy, M.V. (2024) 'Intelligent controller design and fault prediction for renewable energy sources using bi-directional GRU and GEO methods', *Electric Power Components and Systems*, Vol. 52, No. 2, pp.277–291.

Sistani, A., Hosseini, S.A., Sadeghi, V.S. and Taheri, B. (2023) 'Fault detection in a single-bus DC microgrid connected to EV/PV systems and hybrid energy storage using the DMD-IF method', *Sustainability*, Vol. 15, No. 23, p.16269.

Somula, R., Cho, Y. and Mohanta, B.K. (2024) 'SWARAM: osprey optimization algorithm-based energy-efficient cluster head selection for wireless sensor network-based internet of things', *Sensors*, Vol. 24, No. 2, p.521.

Taher, M.A., Behnamfar, M., Sarwat, A.I. and Tariq, M. (2024) 'False data injection attack detection and mitigation using non-linear autoregressive exogenous input-based observers in distributed control for DC microgrid', *IEEE Open Journal of the Industrial Electronics Society*, Vol. 5, pp.441–457.

Veerasamy, V., Abdul Wahab, N.I., Vinayagam, A., Othman, M.L., Ramachandran, R., Inbamani, A. and Hizam, H. (2020) 'A novel discrete wavelet transform-based graphical language classifier for identification of high-impedance fault in distribution power system', *International Transactions on Electrical Energy Systems*, Vol. 30, No. 6, p.e12378.

Wang, Q., Guo, J., Li, R. and Jiang, X.T. (2023) 'Exploring the role of nuclear energy in the energy transition: a comparative perspective of the effects of coal, oil, natural gas, renewable energy, and nuclear power on economic growth and carbon emissions', *Environmental Research*, Vol. 221, p.115290.

Yan, K., Huang, J., Shen, W. and Ji, Z. (2020) 'Unsupervised learning for fault detection and diagnosis of air handling units', *Energy and Buildings*, Vol. 210, p.109689.

Zahraoui, Y., Alhamrouni, I., Mekhilef, S., Basir Khan, M.R., Seyedmahmoudian, M., Stojcevski, A. and Horan, B. (2021) 'Energy management system in microgrids: a comprehensive review', *Sustainability*, Vol. 13, No. 19, p.10492.